Japanese Journal of Applied Physics

The Japan Society of Applied Physics

REGULAR PAPER

Simulation on a non-axisymmetric ring resonator with a nano-antenna for heat-assisted magnetic recording

To cite this article: Jinghan Chen *et al* 2022 *Jpn. J. Appl. Phys.* **61** SK1006

View the article online for updates and enhancements.

You may also like

- Topological hybrid nanocavity for coupling phase transition
Hongyu Zhang, Yanji Zheng, Zhi-Ming Yu et al.
- Numerical analysis of the temperature dependence of near-field polarization for nanoscale thermometry using a triple-tapered near-field optical fiber probe
J Nitta, Y Taguchi, T Saiki et al.
- Nano-plasmonic antennas in the near infrared regime
N Berkovitch, P Ginzburg and M Orenstein

This content was downloaded from IP address 3.144.1.230 on 15/05/2024 at 20:52

Japanese Journal of Applied Physics **61**, SK1006 (2022) **REGULAR PAPER**
https://doi.org/**10.35848/1347-4065/ac6054**

Simulation on a non-axisymmetric ring resonator with a nano-antenna for heat-assisted magnetic recording

Jinghan Chen[1,2], Ryuichi Katayama[1*], and Satoshi Sugiura[3]

[1]*Information Electronics, Graduate School of Engineering, Fukuoka Institute of Technology, Fukuoka 811-0295, Japan*
[2]*School of Science, Nanjing University of Science and Technology, Nanjing, Jiangsu 210094, People's Republic of China*
[3]*InnovaStella, Inc., Bunkyo-ku, Tokyo 113-0032, Japan*

[*]E-mail: r-katayama@fit.ac.jp

Received January 31, 2022; revised March 14, 2022; accepted March 22, 2022; published online June 16, 2022

Heat-assisted magnetic recording is a technology to improve recording density of hard disk drives. The authors' group previously proposed a device, in which a Au nano-antenna as a near-field transducer was attached to a GaAs ring resonator as a light source. The ring resonator should stably oscillate with a single mode to generate near-field light at the tip of the nano-antenna with sufficient energy density. A non-axisymmetric ring resonator structure was proposed this time to improve the energy density and laser oscillation stability. When the decenter between the inner and outer circles of the ring resonator increased, the resonance frequency increased and eigenmodes with higher radial mode order disappeared, which leads to stable laser oscillation. Moreover, when the decenter was 200 or 250 nm, the normalized energy density at the tip of nano-antenna increased 1.2–2.4 times compared with an axisymmetric ring resonator structure while keeping the quality factor to more than 5000.
© 2022 The Japan Society of Applied Physics

1. Introduction

The demand for data storage is expanding nowadays. According to International Data Corporation, the data amount in the world was about 33 ZB in 2018 and is predicted to expand to about 175 ZB in 2025. Therefore, the technologies of data storage need to be greatly improved to increase the storage capacity, for which hard disk drives play an important role. The recording density of hard disk drives means the number of recording marks in a unit square. A recording mark is a small area on a recording medium containing multiple magnetic grains. When all magnetic grains in the area keep the same magnetization in the vertical direction, the area can be seen as bit 0 (upward magnetization) or bit 1 (downward magnetization). The magnetic recording head changes the magnetization of the magnetic grains to write the data. High recording density means small recording marks, so the key to increasing the recording density is to make the recording marks shrink.

However, there are three major factors, that is, signal-to-noise ratio (SNR), thermostability, and writability, that limit the recording density to less than 1 Tb inch^{-2}.[1,2] The SNR is determined by mark shape. Recording marks with smooth edge have a high SNR. Therefore, to form smaller recording marks while satisfying the requirement of high SNR, it is necessary to make the magnetic grains smaller. However, the thermostability becomes lower because it is difficult for smaller magnetic grains to keep their magnetization. The recording medium must have a higher coercivity to improve the thermostability, but it reduces the writability. To break through this trilemma, many new methods have been proposed. Among them, heat-assisted magnetic recording (HAMR) has been attracting extensive attention of academia and industry.[3–7]

The purpose of HAMR is to deal with the difficulty in writing the data with a limited magnetic field intensity obtained by a magnetic recording head. The coercivity of the recording medium is reduced by heating it locally with a light spot during recording, which makes it possible to write the data with a limited magnetic field intensity. The coercivity of the recording medium recovers to a high level after the light spot moves to the next position, which makes it possible to store the data stably. The HAMR system consists of a light delivery system, a magnetic recording head, a head-disk interface, and a recording medium.

The most significant problem that HAMR technology faces is the formation of the light spot. In order to achieve more than 1 Tb inch^{-2} recording density, the area occupied by each recording mark needs to be smaller than 25 nm × 25 nm. To heat such a small area requires a corresponding small light spot, which is difficult to achieve with ordinary far-field optics because of the diffraction limit determined by the wavelength of the laser and numerical aperture of the lens. The popular solution is to introduce a near-field transducer (NFT) to apply near-field optics to make the spot size approach 10 nm or less.[5] The NFTs make use of apertures,[8] antennas,[9] or a combination thereof. An external light couples with the NFT and excites localized surface plasmons[10–12] to generate a near-field light, which heats the small area on the recording medium. As the examples of NFTs, Lollipop,[5] E-antenna,[6] and beaked-plate[13] types were proposed earlier. However, in these NFTs, the light source is usually separated, so that there are lots of losses during light delivery and device size is large.

Kuriyama et al. proposed a mesa-type device for a HAMR heater.[14] In this device, a metal nano-dot as the NFT is put at the top of a semiconductor mesa, which is doped with quantum dots (QDs),[15,16] as a light source. The nano-dot is excited by the light that the mesa produced to generate a near-field light at the top of nano-dot. Katayama et al. analyzed the near-field light generated by the nano-dot,[17] simulated the characteristics of near-field light when the materials of nano-dot and mesa were changed,[18,19] and then proposed a ring-resonator-type device.[20] The structure of this device is shown in Fig. 1. A metal nano-antenna as the NFT is attached to the side of a semiconductor ring resonator doped with QDs as a light source. The ring resonator produces light that excites the nano-antenna to generate a near-field light at the tip of nano-antenna. In both types of devices, the loss during light delivery can be minimized and

 © 2022 The Japan Society of Applied Physics

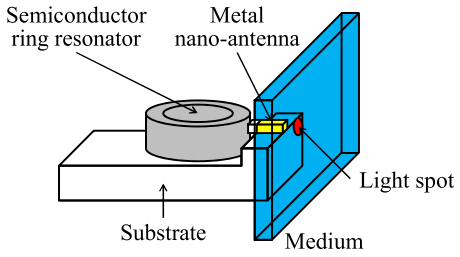

Fig. 1. (Color online) Structure of proposed device.

device size can be small because the light source is integrated. Moreover, the ring-resonator-type device is superior to the mesa-type device in terms of efficiency, practicability, and manufacturability.

In the ring-resonator-type device, the ring resonator has a double-hetero-structure in the vertical direction. If an electric current is injected to the ring resonator, it acts as a laser whose electric field is confined in the micro-ring[21–24] as a whispering gallery mode (WGM). Generally, a WGM microcavity features a high-quality factor.[25,26] In the WGM microcavity, the light propagates in a two-dimensional plane with continuous total internal reflection at the outer boundary of the microcavity without being refracted out of the microcavity. The light is confined in the direction perpendicular to the plane by another structure. The shape of general WGM microcavity is circular or polygonal. Several common WGM microcavities include micro-sphere,[27] micro-disk,[28] and micro-toroid.[29] Among them, micro-ring or micro-disk is a good choice for an integrated light source because of its planarity.

The authors' group simulated the eigenmodes, resonance frequency, electric field distribution, and energy density at the tip of nano-antenna of the device before.[30] It was found that when the ring width became narrower, the normalized energy density at the tip of nano-antenna increased and unnecessary eigenmodes that make the laser oscillation unstable disappeared. However, the resonance frequency became more sensitive to the ring width, which determined the lower limit of ring width. A non-axisymmetric ring resonator structure was proposed to improve the energy density and laser oscillation stability.[31] In this paper, more simulation was conducted and more discussion was made especially on the unnecessary eigenmodes compared with Ref. 31.

2. Simulation methods

The simulation model is shown in Fig. 2. The ring resonator has a GaAs active layer doped with InAs QDs and sandwiched between two AlGaAs cladding layers. A Au nano-antenna is attached to the active layer via a SiO_2 spacer. The center of inner circle O1 is offset from that of outer circle O2 along the x-direction. The decenter is expressed as D. When D is positive and negative, the ring resonator near the nano-antenna is narrow and wide, respectively.

The materials and refractive indices of the device are summarized in Table I, and the dimensions of the device are summarized in Table II. The amount of D was varied from -350 to 350 nm to figure out how D affects the resonance frequency of the eigenmodes, energy density at the tip of nano-antenna, and quality factor of the ring resonator. When

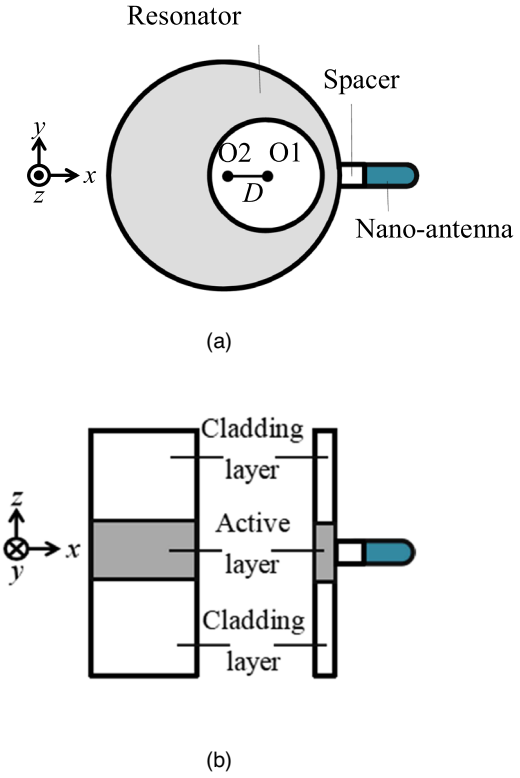

Fig. 2. (Color online) Simulation model: (a) plane view and (b) side view.

Table I. Materials and refractive indices of device.

	Materials	Refractive indices
Active layer	GaAs	3.5
Cladding layer	AlGaAs	3.1
Nano-antenna	Au	$0.28 + 7.2i$
Spacer	SiO_2	1.5

Table II. Dimensions of device.

Decenter of inner circle	D (varied)
Inner diameter of resonator	1000 nm
Outer diameter of resonator	2000 nm
Thickness of active layer	200 nm
Diameter of nano-antenna	50 nm
Length of nano-antenna	100 nm
Thickness of spacer	50 nm

$D = -350$ nm, the width of the part of ring resonator near the nano-antenna was 850 nm, and when $D = 350$ nm, the width of the part of ring resonator near the nano-antenna was 150 nm. The center wavelength (frequency) of laser gain determined by the QDs was 1050 nm (285.5 THz). The resonance frequency was calculated within the range of 270–305 THz considering the laser gain. The finite element method was used for the calculation.

For the ring resonator as a WGM microcavity, the lights propagating clockwise and counterclockwise interfere with each other and form a stable standing wave in the tangential direction. The standing wave constantly interacts with the QDs and generates stimulated emission. The eigenmodes correspond to the electric field distributions that exist in the cavity. The modes in the tangential direction are called tangential modes. As there are also reflections at the inner

© 2022 The Japan Society of Applied Physics

and outer boundaries of the cavity in the radial direction, a standing wave is formed in the radial direction also. The modes in the radial direction are called radial modes. The number of eigenmodes is determined by the width, size, and refractive index of the ring resonator. The tangential mode order is expressed by m. A larger cavity leads to solutions with larger m values. Meanwhile, the radial mode order is expressed by l. The eigenmodes can be further classified into TE-like and TM-like modes. The former and the latter are dominated by radial and vertical component of the electric field, respectively.

3. Simulation results

An example of electric field intensity distribution of TM-like mode when $D = 0$ nm is shown in Fig. 3. Only the region in which $y > 0$ and $z > 0$ is shown. There are 15 intensity peaks in the tangential direction, which means $m = 15$, and there is only one intensity peak in the radial direction, which means $l = 1$. An example of electric field intensity distribution of TE-like mode when $D = 0$ nm is shown in Fig. 4. There are 15 intensity peaks in the tangential direction, which means $m = 15$, and there is only one intensity peak in the radial direction, which means $l = 1$. There was no near-field light at the tip of nano-antenna in Figs. 3(c) and 3(d), while there was a certain amount of near-field light at the tip of nano-antenna in Figs. 4(c) and 4(d). These results confirmed that only TE-like mode can generate near-field light. An example of electric field intensity distribution of TM-like mode with higher radial mode order when $D = 0$ nm is shown in Fig. 5. There are 12 intensity peaks in the tangential direction, which means $m = 12$, and there are two intensity peaks in the radial direction, which means $l = 2$. An example of electric field intensity distribution of TE-like mode with higher radial mode order when $D = 0$ nm is shown in Fig. 6. There are 11 intensity peaks in the tangential direction, which means $m = 11$, and there are two intensity peaks in the radial direction, which means $l = 2$.

Figure 7(a) shows an example of electric field intensity distribution of the TE-like mode with $l = 1$ when $D = 0$ nm, and Fig. 7(b) shows an example of electric field intensity distribution of TE-like mode with $l = 1$ when $D = 350$ nm. For both examples, there are 14 intensity peaks in the tangential direction, which means $m = 14$. In Fig. 7(a), the intensity peaks were uniformly spaced in the tangential direction, and the electric field was mostly confined into the ring in the radial direction. On the other hand, in Fig. 7(b), the interval between adjacent intensity peaks in the tangential direction increased as the ring became narrower, and the electric field spread out of the ring in the radial direction when the ring became narrower. Moreover, although the electric field intensity in the ring resonator in Fig. 7(b) was lower than that in Fig. 7(a), the electric field intensity at the tip of nano-antenna in Fig. 7(b) was higher than that in Fig. 7(a). Regarding the TE-like mode with higher radial mode order, there were no solutions when $D = 350$ nm.

Figure 8 shows the dependence of resonance frequency on D for TM-like mode with $l = 1$. There were two solutions with $m = 15$ and 16 within the laser gain range. Figure 9 shows the dependence of resonance frequency on D for TE-like mode with $l = 1$. There were two solutions with $m = 14$ and 15 within the laser gain range. In both Figs. 8 and 9, the resonance frequency increased as the absolute value of D increased, especially when the absolute value of D was more than 200 nm. However, the resonance frequency for TE-like mode was less tolerant against the increase in absolute value of D compared with that for the TM-like mode. In Fig. 8, the increase in resonance frequency when $D = 350$ nm was only about 2 THz. On the other hand, in Fig. 9, the increase in resonance frequency when $D = 350$ nm was about 13–14 THz, but the resonance frequency was still within the laser gain range.

The dependence of normalized energy density at the tip of nano-antenna on D for TE-like mode with $l = 1$ is shown in Fig. 10. The normalized energy density drastically increased

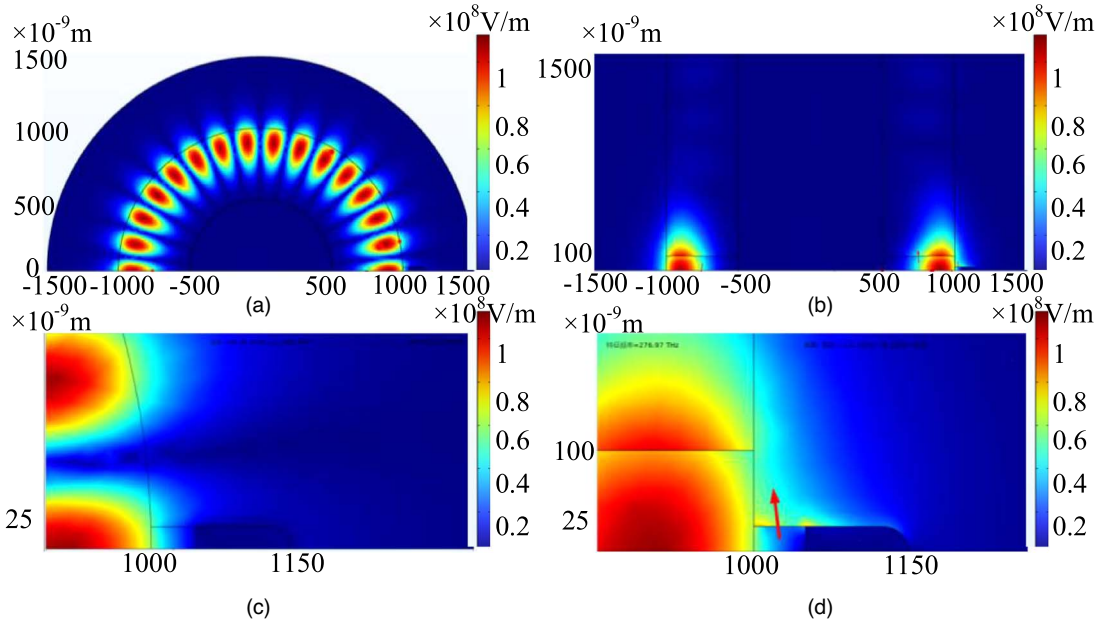

Fig. 3. (Color online) Example of electric field intensity distribution of TM-like mode when $D = 0$ nm: (a) x–y plane, (b) x–z plane, (c) enlarged view of (a) around nano-antenna, and (d) enlarged view of (b) around nano-antenna.

© 2022 The Japan Society of Applied Physics

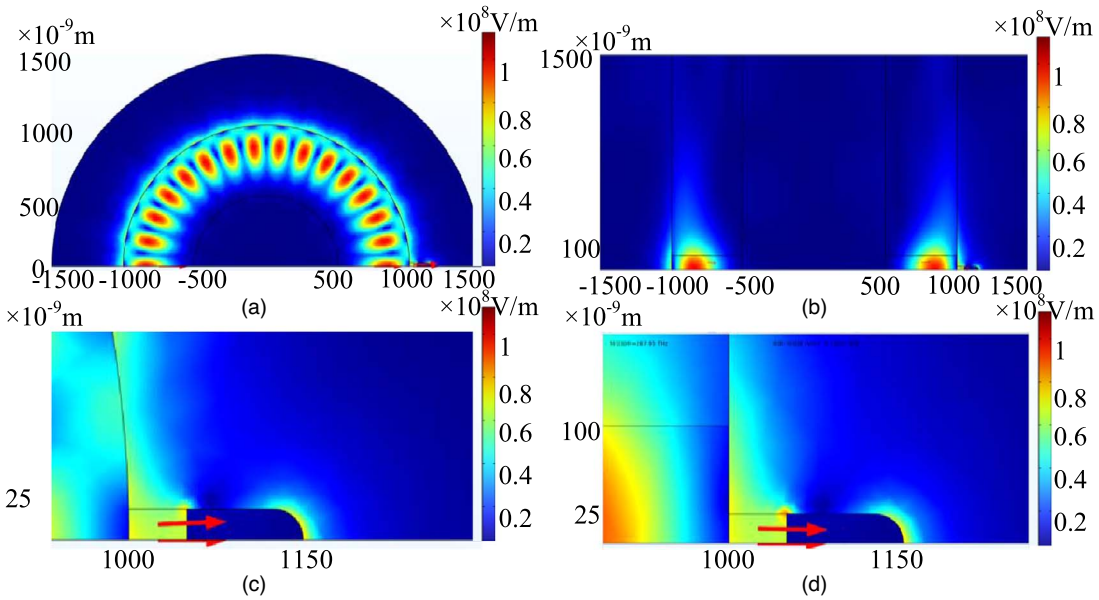

Fig. 4. (Color online) Example of electric field intensity distribution of TE-like mode when $D = 0$ nm: (a) x–y plane, (b) x–z plane, (c) enlarged view of (a) around nano-antenna, and (d) enlarged view of (b) around nano-antenna.

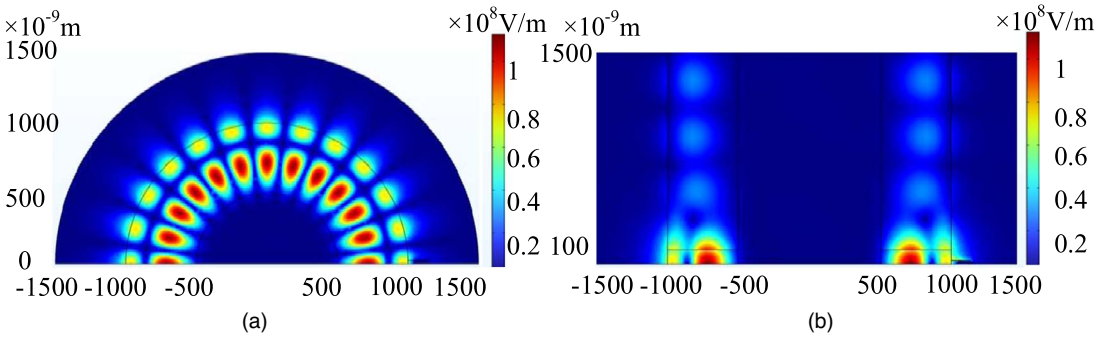

Fig. 5. (Color online) Example of electric field intensity distribution of TM-like mode with higher radial mode order when $D = 0$ nm: (a) x–y plane and (b) x–z plane.

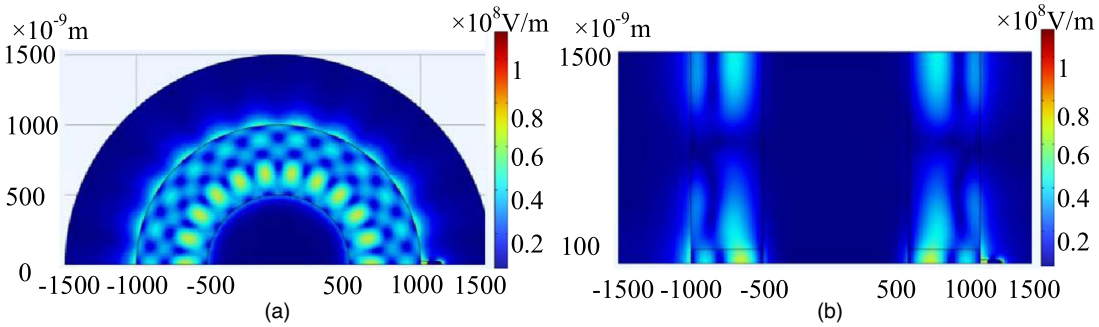

Fig. 6. (Color online) Example of electric field intensity distribution of TE-like mode with higher radial mode order when $D = 0$ nm: (a) x–y plane and (b) x–z plane.

as D increased to more than 250 nm, which coincides with the electric field intensity distributions shown in Figs. 7(a) and 7(b). The normalized energy density with $m = 14$ when $D = 350$ nm was 27 times higher than that when $D = 0$ nm, and the normalized energy density with $m = 15$ when $D = 350$ nm was 21 times higher than that when $D = 0$ nm.

The dependence of resonance frequency on D for TM-like mode with $l = 2$ is shown in Fig. 11. There were two solutions with $m = 11$ and 12 within the laser gain range. The dependence of resonance frequency on D for TE-like mode with $l = 2$ is shown in Fig. 12. There were two solutions with $m = 10$ and 11 within the laser gain range. In both Figs. 11 and 12, the resonance frequency increased as the absolute value of D increased. However, the resonance frequency for TE-like mode was less tolerant against the increase in absolute value of D compared with that for TM-like mode. These tendencies were the same as those with $l = 1$.

The dependence of quality factor of the ring resonator on D for TE-like mode with $l = 1$ is shown in Fig. 13. The results for two solutions ($m = 14$ and 15) are shown. For both

© 2022 The Japan Society of Applied Physics

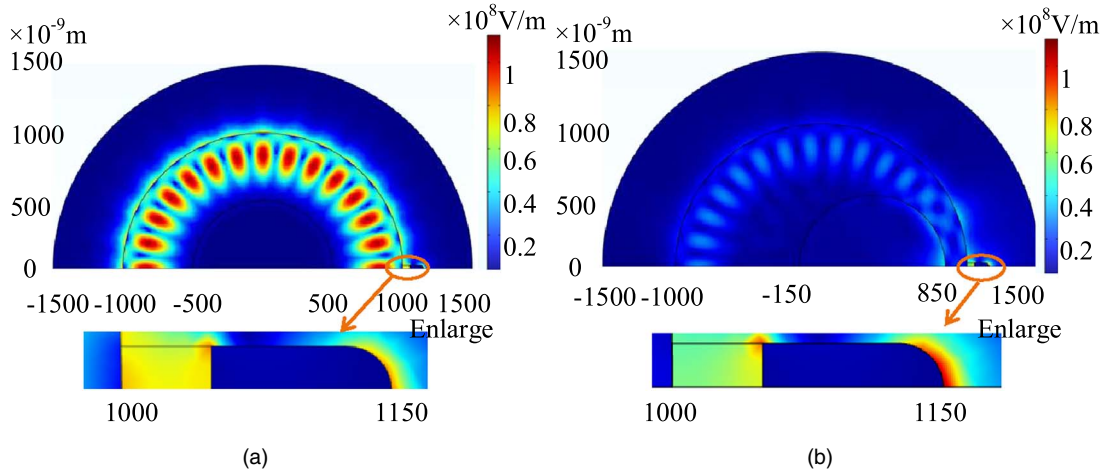

Fig. 7. (Color online) Examples of electric field intensity distribution of TE-like mode for different D values: (a) $D = 0$ nm and (b) $D = 350$ nm.

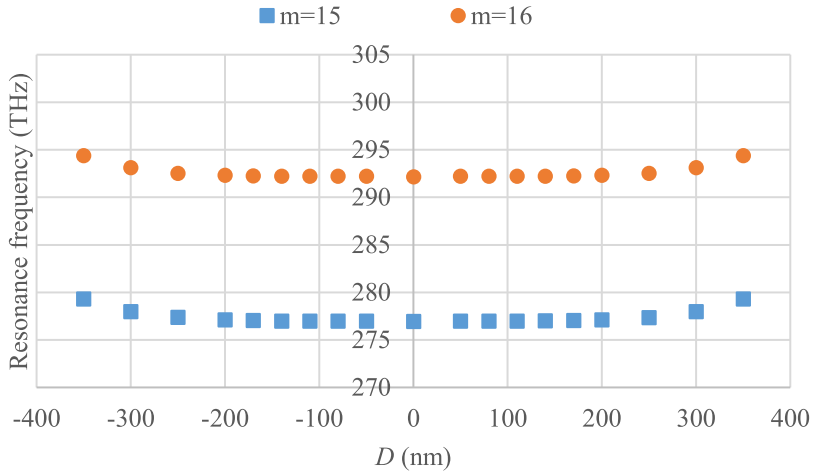

Fig. 8. (Color online) Dependence of resonance frequency on D for TM-like mode with $l = 1$.

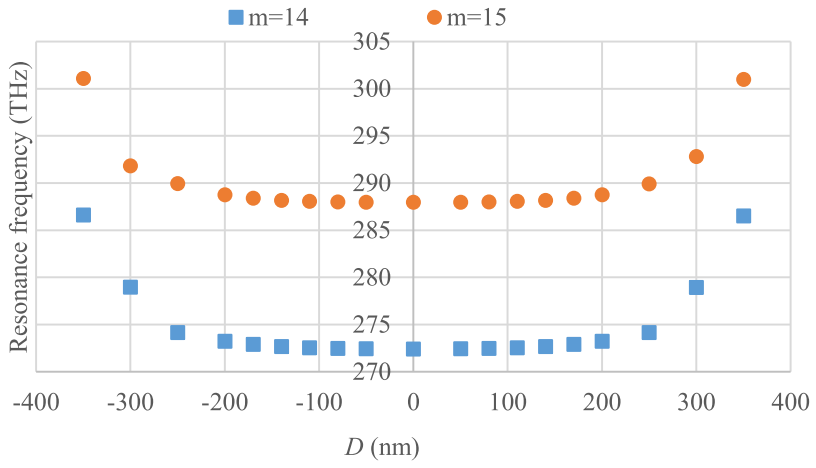

Fig. 9. (Color online) Dependence of resonance frequency on D for TE-like mode with $l = 1$.

solutions, the quality factor decreased as the absolute value of D increased. However, the quality factor with $m = 14$ and 15 was more than 5000 when the absolute value of D was less than 200 and 250 nm, respectively. Moreover, the energy confined in the ring resonator divided by total energy was defined as energy confinement ratio, and the dependence of energy confinement ratio on D for TE-like mode with $l = 1$ is shown in Fig. 14. For simplicity, the calculation was done only when D was positive. The results for two solutions ($m = 14$ and 15) are shown. For both solutions, the energy confinement ratio gradually decreased as D increased from 0 to 300 nm and noticeably decreased when D was 350 nm.

4. Discussion

As shown in Figs. 3 and 4, only the TE-like mode can generate near-field light at the tip of nano-antenna. For the TE-like mode, the direction of electric field is parallel to the axial direction of nano-antenna. This electric field makes the

© 2022 The Japan Society of Applied Physics

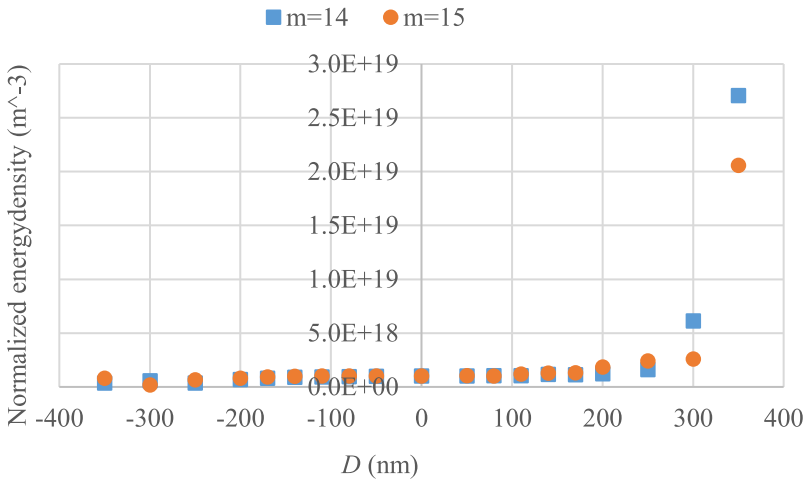

Fig. 10. (Color online) Dependence of normalized energy density at the tip of nano-antenna on D for TE-like mode with $l = 1$.

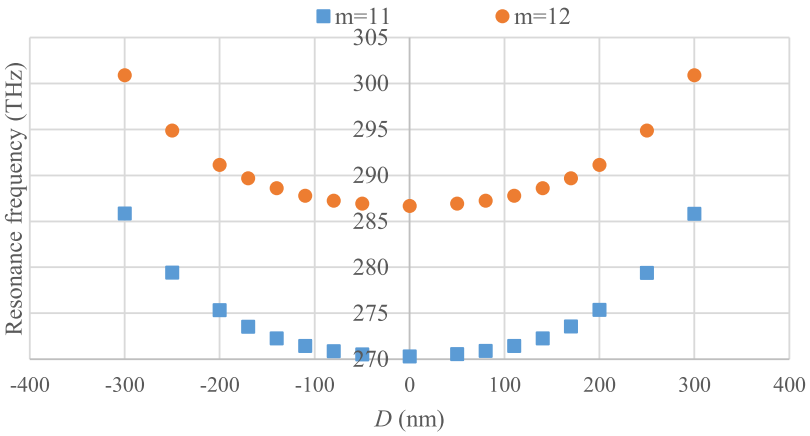

Fig. 11. (Color online) Dependence of resonance frequency on D for TM-like mode with $l = 2$.

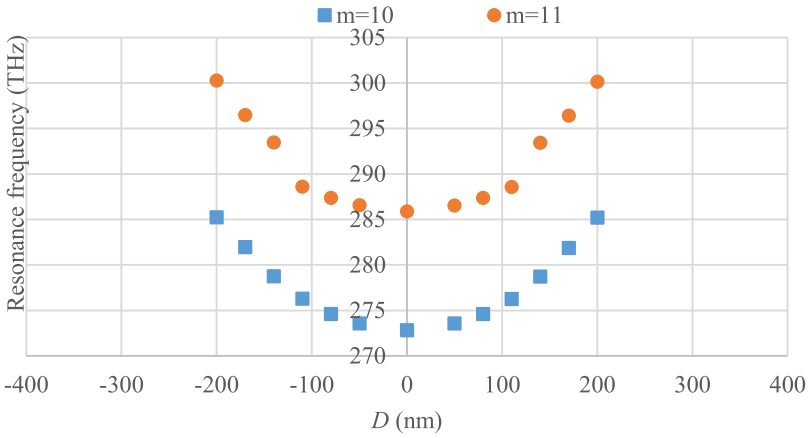

Fig. 12. (Color online) Dependence of resonance frequency on D for TE-like mode with $l = 2$.

free electrons in the nano-antenna oscillate thereby forming an electric dipole in the axial direction of nano-antenna. This oscillation is called localized surface plasmons and excites near-field light at the tip of nano-antenna.

In Fig. 7(b), the interval between adjacent intensity peaks in the tangential direction increased as the ring became narrower. This is because the effective refractive index became lower as the ring became narrower. The effective refractive index has a value between the refractive index of ring resonator and that of air. As the ring became narrower, the contribution of air increased and the effective refractive index became closer to the refractive index of air. The wavelength of light in the ring resonator is given by the wavelength of light in vacuum divided by the effective refractive index. Therefore, as the effective refractive index became lower, the wavelength of light in the ring resonator became longer. As a result, the interval between adjacent intensity peaks in the tangential direction increased. Moreover, in Fig. 7(b), the electric field spread out of the ring in the radial direction when the ring became narrower.

© 2022 The Japan Society of Applied Physics

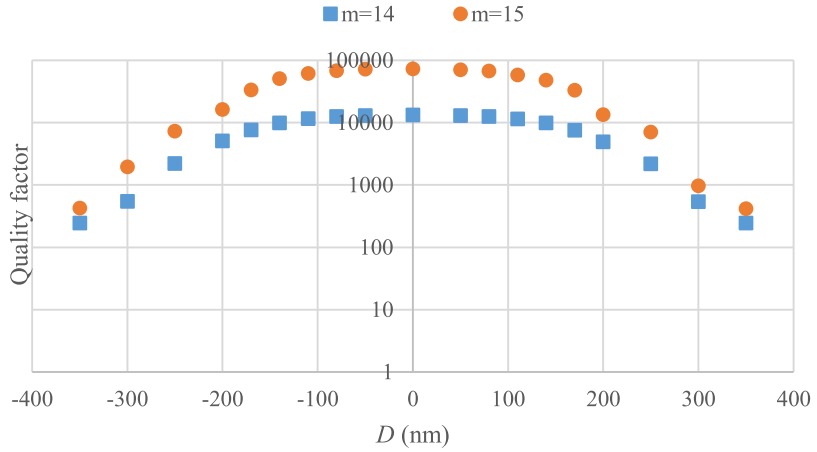

Fig. 13. (Color online) Dependence of quality factor on D for the TE-like mode with $l = 1$.

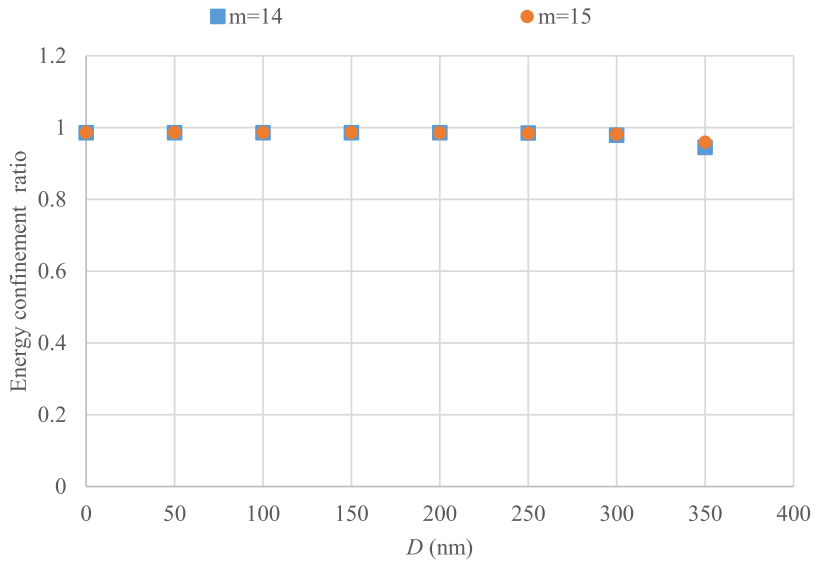

Fig. 14. (Color online) Dependence of energy confinement ratio on D for the TE-like mode with $l = 1$.

This is because the range of electric field in the radial direction became wider than the ring width when the ring became narrower.

The resonance frequency f is expressed as

$$f = \frac{mc}{2\pi r_{\text{eff}} n_{\text{eff}}}, \tag{1}$$

where r_{eff} is the effective radius of light propagation path, n_{eff} is the effective refractive index, and c is the velocity of light in vacuum. The denominator of the fraction is circular optical path length in the ring resonator. As shown in Figs. 8 and 9, the resonance frequency for a larger m value was higher than that for a smaller m value. This is easily understood from Eq. (1).

Comparing Figs. 8 and 9 for the same m value, the resonance frequency for the TE-like mode was higher than that for the TM-like mode. This is also understood from Eq. (1), considering the difference in r_{eff} between the two modes. The reason why the resonance frequency increased as the absolute value of D increased is that n_{eff} became lower as the absolute value of D increased. As the ring became narrower, n_{eff} became lower because the contribution of air increased. On the other hand, as the ring became wider, n_{eff} did not become higher so much because the contribution of air did not decrease so much. As a result, as the absolute value of D increased, n_{eff} averaged in the entire circumference became lower. As shown in Figs. 3 and 4, the range of electric field in the radial direction for the TE-like mode was wider than that for TM-like mode. Therefore, as the absolute value of D increased, the electric field for the TE-like mode spread out of the ring in the radial direction earlier than that for TM-like mode. This is the reason why the resonance frequency for the TE-like mode was less tolerant against the increase in absolute value of D compared with that for TM-like mode. When the absolute value of D becomes too large, the intensity peak of the electric field in the radial direction spreads out of the ring and the corresponding eigenmode disappears.

As for the normalized energy density shown in Fig. 10, when D becomes large, more electric field spreads out of the ring and is coupled to the nano-antenna. This is the reason why the normalized energy density drastically increased as D increased to more than 250 nm.

The m values for $l = 2$ modes shown in Figs. 11 and 12 were smaller than those for $l = 1$ modes shown in Figs. 8 and 9. This is also understood from Eq. (1), considering the difference in r_{eff} between $l = 1$ and 2 modes. Moreover, as the absolute value of D increased, $l = 2$ modes disappeared

© 2022 The Japan Society of Applied Physics

earlier than $l = 1$ modes did. This is because the range of electric field in the radial direction for $l = 2$ modes was wider than that for $l = 1$ modes. This leads to stable laser oscillation because of the suppression of mode competition between modes with different l values. Now let us consider the solutions with $l = 1$. For the TE-like mode, there were two solutions with $m = 14$ and 15 as shown in Fig. 9. When D was 200 or 250 nm, their resonance frequencies were about 274 and 289 THz, respectively. When D was 350 nm, their resonance frequencies were about 286 and 301 THz, respectively. On the other hand, for TM-like mode, there were two solutions with $m = 15$ and 16 as shown in Fig. 8. When D was 200 or 250 nm, their resonance frequencies were about 277 and 292 THz, respectively. When D was 350 nm, their resonance frequencies were about 279 and 294 THz, respectively. If the center frequency of laser gain would be 285.5 THz, the TE-like mode with $m = 15$ would be easier to be selected when D is 200 or 250 nm, and the TE-like mode with $m = 14$ would be easier to be selected when D is 350 nm. In each case, the laser would stably oscillate with single mode. In addition, the normalized energy density would be high when D is 200 or 250 nm and very high when D is 350 nm.

The objective of research was to improve the energy density and laser oscillation stability of the ring-resonator-type device. This can be achieved not only by making the ring resonator non-axisymmetric but also by making the ring width narrower in the entire circumference as described in Ref. 30. However, in the latter case, as the ring width became narrower, the resonance frequency increased more drastically than in the former case because n_{eff} became lower in the entire circumference. As a result, the lower limit of ring width where necessary eigenmode disappeared was about 200–300 nm, and the improvement in normalized energy density was not so significant. On the other hand, in the former case, it was possible to make the ring width at the bottom of nano-antenna as narrow as 150 nm while keeping the resonance frequency within the laser gain range, and significant improvement in normalized energy density was achieved.

As for the quality factor shown in Fig. 13, it affects the lasing characteristics of ring resonator. According to Ref. 32, when the quality factor is less than 1000, the laser cannot work due to high threshold current, and when the quality factor is more than 5000, it hardly affects the threshold current. If the minimum allowable quality factor of the ring resonator is determined to be 5000, the maximum allowable value of D with $m = 14$ and 15 was 200 and 250 nm, respectively. The normalized energy density with $m = 14$ when $D = 200$ nm was 1.2 times higher than that when $D = 0$ nm, and the normalized energy density with $m = 15$ when $D = 250$ nm was 2.4 times higher than that when $D = 0$ nm. Although these values were smaller than those when $D = 350$ nm, the non-axisymmetric ring resonator structure was still found to be effective for improving the energy density at the tip of nano-antenna. As for the energy confinement ratio shown in Fig. 14, it is understood that more energy leaked from the ring resonator to air as D increased, although most of the energy was still confined in the ring resonator. This is considered to be the reason for the decrease in the quality factor. Moreover, the energy confinement ratio with $m = 14$ was slightly smaller than that with $m = 15$. This corresponds to the fact that the quality factor with $m = 14$ was lower than that with $m = 15$.

The absolute magnitude of the energy density at the tip of nano-antenna is determined not only by the transmission efficiency of optical energy from the ring resonator to the nano-antenna but also by the conversion efficiency from electrical energy to optical energy at the ring resonator. The former can be calculated through wave optics simulation and the latter can be calculated through semiconductor simulation. Since this research focused on the former, the research on the latter will be the next step.

5. Conclusions

In the ring-resonator-type device for HAMR, the ring resonator to generate near-field light at the tip of nano-antenna should be stable and easy to manufacture. Moreover, the near-field light should have energy density that is high enough to heat the recording medium. In this research, a non-axisymmetric ring resonator structure was proposed for this purpose. The authors simulated the eigenmodes, resonance frequency, electric field intensity distribution, and energy density at the tip of the nano-antenna when the decenter between inner and outer circles of the ring resonator (D) was varied from -350 to 350 nm.

The near-field light was generated only for the TE-like mode. The resonance frequency increased as the absolute value of D increased. For $l = 1$ modes, the resonance frequency increased especially when the absolute value of D was more than 200 nm, but it was still within the laser gain range. On the other hand, $l = 2$ modes disappeared earlier as the absolute value of D increased. When D is 200 or 250 nm, the TE-like mode with $m = 15$ would be easier to be selected, and when D is 350 nm, the TE-like mode with $m = 14$ would be easier to be selected. In each case, the laser would stably oscillate with a single mode. Moreover, when the decenter was 200–250 nm, the normalized energy density at the tip of nano-antenna increased 1.2–2.4 times compared with an axisymmetric ring resonator structure while keeping the quality factor to more than 5000.

Acknowledgments

This work was supported by JSPS KAKENHI Grant Number JP19K04541.

1) H. N. Bertram and M. Williams, IEEE Trans. Magn. **36**, 4 (2000).
2) D. Weller and A. Moser, IEEE Trans. Magn. **35**, 4423 (1999).
3) M. H. Kryder, E. C. Gage, T. W. McDaniel, W. A. Challener, R. E. Rottmayer, G. Ju, Y.-T. Hsia, and M. F. Erden, Proc. IEEE **96**, 1810 (2008).
4) H. Saga, H. Nemoto, H. Sukeda, and M. Takahashi, Jpn. J. Appl. Phys. **38**, 1839 (1999).
5) W. A. Challener et al., Nat. Photonics **3**, 220 (2009).
6) B. C. Stipe et al., Nat. Photonics **4**, 484 (2010).
7) A. Q. Wu et al., IEEE Trans. Magn. **49**, 779 (2013).
8) D. W. Pohl, W. Denk, and M. Lanz, Appl. Phys. Lett. **44**, 651 (1984).
9) P. Bharadwaj, B. Deutsch, and L. Novotny, Adv. Opt. Photonics **1**, 438 (2009).
10) S. Link S and M. A. El-Sayed, J. Phys. Chem. B **103**, 8410 (1999).
11) S. Link, Z. L. Wang, and M. A. El-Sayed, J. Phys. Chem. B **104**, 7867 (2000).
12) L. Novotny and N. van Hulst, Nat. Photonics **5**, 83 (2011).
13) T. Matsumoto, Y. Anzai, T. Shintani, K. Nakamura, and T. Nishida, Opt. Lett. **31**, 259 (2006).

© 2022 The Japan Society of Applied Physics

14) K. Kuriyama, M. J. Chabalko, Y. Kong, Y. Luo, T. E. Schlesinger, and J. A. Bain, IEEE Trans. Magn. **49**, 3560 (2013).
15) T. Kawazoe, K. Kobayashi, and M. Ohtsu, Appl. Phys. Lett. **86**, 103102 (2005).
16) T. Kawazoe, M. Ohtsu, S. Aso, Y. Sawado, Y. Hosoda, K. Yoshikawa, K. Akahane, N. Yamamoto, and M. Naruse, Appl. Phys. B **103**, 537 (2011).
17) R. Katayama, J. Appl. Phys. **115**, 17B728 (2014).
18) R. Katayama, Opt. Rev. **21**, 568 (2014).
19) R. Katayama, T. Kasuya, S. Sugiura, and K. Yoshizawa, Jpn. J. Appl. Phys. **54**, 09MG01 (2015).
20) R. Katayama and S. Sugiura, Jpn. J. Appl. Phys. **58**, SKKB01 (2019).
21) A. S.-H. Liao and S. Wang, Appl. Phys. Lett. **36**, 801 (1980).
22) T. Krauss, P. J. R. Laybourn, and J. Roberts, Electron. Lett. **26**, 2095 (1990).
23) S. Oku, M. Okayasu, and M. Ikeda, IEEE Photonics Technol. Lett. **3**, 588 (1991).
24) J. P. Hohimer, D. C. Craft, G. R. Hadley, G. A. Vawter, and M. E. Warren, Appl. Phys. Lett. **59**, 3360 (1991).
25) R. D. Richtmyer, J. Appl. Phys. **10**, 391 (1939).
26) V. B. Braginsky, M. L. Gorodetsky, and V. S. Ilchenko, Phys. Lett. A **137**, 393 (1989).
27) R. E. Benner, P. W. Barber, J. F. Owen, and R. K. Chang, Phys. Rev. Lett. **44**, 475 (1980).
28) S. L. McCall, A. F. J. Levi, R. E. Slusher, S. J. Pearton, and R. A. Logan, Appl. Phys. Lett. **60**, 289 (1992).
29) D. K. Armani, T. J. Kippenberg, S. M. Spillane, and K. J. Vahala, Nature **421**, 925 (2003).
30) J. Chen, R. Katayama, and S. Sugiura, Opt. Rev. **28**, 681 (2021).
31) J. Chen, R. Katayama, and S. Sugiura, Presented at Microoptics Conf., 2021, PO-14.
32) Y. Xiong, T. Umeda, X. Zhang, M. Morifuji, H. Kajii, A. Maruta, and M. Kondow, IEEE J. Sel. Top. Quantum Electron. **24**, 4900207 (2018).

© 2022 The Japan Society of Applied Physics